

# A Novel MYCN-Specific Antigen Oligonucleotide Deregulates Mitochondria and Inhibits Tumor Growth in MYCN-Amplified Neuroblastoma



Luca Montemurro<sup>1</sup>, Salvatore Raieli<sup>2</sup>, Silvia Angelucci<sup>1</sup>, Damiano Bartolucci<sup>1</sup>, Camilla Amadesi<sup>2</sup>, Silvia Lampis<sup>2</sup>, Anna Lisa Scardovi<sup>2</sup>, Leonardo Venturelli<sup>2</sup>, Giammario Nieddu<sup>2</sup>, Lucia Cerisoli<sup>2</sup>, Matthias Fischer<sup>3,4</sup>, Gabriella Teti<sup>5</sup>, Mirella Falconi<sup>5</sup>, Andrea Pession<sup>1</sup>, Patrizia Hrelia<sup>6</sup>, and Roberto Tonelli<sup>6</sup>

## Abstract

Approximately half of high-risk neuroblastoma is characterized by MYCN amplification. N-Myc promotes tumor progression by inducing cell growth and inhibiting differentiation. MYCN has also been shown to play an active role in mitochondrial metabolism, but this relationship is not well understood. Although N-Myc is a known driver of the disease, it remains a target for which no therapeutic drug exists. Here, we evaluated a novel MYCN-specific antigen PNA oligonucleotide (BGA002) in MYCN-amplified (MNA) or MYCN-expressing neuroblastoma and investigated the mechanism of its antitumor activity. MYCN mRNA and cell viability were reduced in a broad set of neuroblastoma cell lines following BGA002 treatment. Furthermore, BGA002 decreased N-Myc protein levels and apoptosis in MNA neuroblastoma. Analysis of gene expression data from patients with neuroblastoma revealed that MYCN was associated with increased reactive oxygen species (ROS), downregulated mitophagy, and poor prognosis. Inhibition of MYCN caused profound mitochon-

drial damage in MNA neuroblastoma cells through downregulation of the mitochondrial molecular chaperone TRAP1, which subsequently increased ROS. Correspondingly, inhibition of MYCN reactivated mitophagy. Systemic administration of BGA002 downregulated N-Myc and TRAP1, with a concomitant decrease in MNA neuroblastoma xenograft tumor weight. In conclusion, this study highlights the role of N-Myc in blocking mitophagy in neuroblastoma and in conferring protection to ROS in mitochondria through upregulation of TRAP1. BGA002 is a potentially improved MYCN-specific antigen oligonucleotide that reverts N-Myc-dysregulated mitochondrial pathways, leading to loss of the protective effect of N-Myc against mitochondrial ROS.

**Significance:** A second generation antigen peptide oligonucleotide targeting MYCN induces mitochondrial damage and inhibits growth of MYCN-amplified neuroblastoma cells.

## Introduction

Neuroblastoma is the deadliest pediatric tumor. While patients with a low or intermediate risk have a favorable outcome, the high-risk group has a survival rate below 50% (1). The latter group often presents with MYCN amplification (50% of the high-risk

group; ref. 2). N-Myc is a well-known driver of the disease (3) and is strongly associated with poor survival prognosis (4, 5). N-Myc promotes cell growth, inhibits cell differentiation while maintaining a stem-like phenotype; its levels correlate with metastasis and the induction of angiogenesis (6, 7). Furthermore, MYCN overexpression affects metabolism to support the higher energy demand of the tumor cells (8–10). Beyond increasing glycolysis and glutaminolysis, N-Myc is involved in mitochondrial functional alteration; however, the mechanism of this effect is not fully understood (11).

Interestingly, MYCN is expressed during embryogenesis and is virtually absent during adulthood (12). All these factors make N-Myc a promising target for neuroblastoma therapy. However, in order for an inhibitor to be effective, it should either interfere with the N-Myc/MAX heterodimers, or with N-Myc interaction with DNA, without inhibiting the highly homologous myc. These requirements have led to N-Myc being currently considered an unlikely target for therapeutic intervention (13).

Although indirect therapeutic approaches in combating neuroblastoma by inhibiting N-Myc have been proposed, considering the broad role of MYCN in neuroblastoma and the lack of a complete understanding of its mechanism, the challenge still remains. Given the difficulties encountered in developing a small-molecule inhibitor, other approaches including the use of

<sup>1</sup>Interdepartmental Center for Cancer Research, University of Bologna, Bologna, Italy. <sup>2</sup>R&D Department, BIOGENERA SpA, Bologna, Italy. <sup>3</sup>Department of Experimental Pediatric Oncology, University Children's Hospital of Cologne, Medical Faculty, Cologne, Germany. <sup>4</sup>Center for Molecular Medicine Cologne (CMMC), University of Cologne, Cologne, Germany. <sup>5</sup>Department of Biomedical and Neuromotor Sciences-DBNS, University of Bologna, Bologna, Italy. <sup>6</sup>Department of Pharmacy and Biotechnologies, University of Bologna, Bologna, Italy.

**Note:** Supplementary data for this article are available at Cancer Research Online (<http://cancerres.aacrjournals.org/>).

L. Montemurro and S. Raieli contributed equally to this article.

**Corresponding Author:** Roberto Tonelli, University of Bologna, Irnerio Street 48, Bologna 40100, Italy. Phone: 39-051-20-9-1784; E-mail: roberto.tonelli@unibo.it

Cancer Res 2019;79:6166–77

doi: 10.1158/0008-5472.CAN-19-0008

©2019 American Association for Cancer Research.



Cytometer (Beckman Coulter). The data were analyzed with FlowJo Software (Tree Star).

#### Mitochondrial net analysis

Kelly ( $6 \times 10^4$  cells) were seeded on  $12 \times 12$  mm circular glass in a 24-well plate for 24 hours in Opti-MEM medium, treated with  $5 \mu\text{mol/L}$  BGA002 or  $50 \text{ nmol/L}$  TRAP1 siRNA with the addition of 4% FBS 6 hours after treatment. At the end of the treatment, MitoTracker Deep RedFM (M22426; Thermo Fisher Scientific) was added according to the manufacturer's instructions. Cells were fixed with 4% PFA and were mounted on a glass slide with SlowFade Diamond Antifade Mountant (S36967; Thermo Fisher Scientific). Images were acquired with a confocal microscope (Leica TCS LS). ImageJ was used to capture the images. Briefly, the signal was reduced with a subtraction command with a value of 25, and the images were convolved with a Gaussian blur ( $\sigma = 1$ ).

#### Transmission electron microscopy

Kelly cells were seeded onto a  $24 \times 24$  mm square glass support in a 6-well plate overnight. PNA oligo treatment was performed as described above. Tet21N cells, cultured for at least 72 hours with or without tetracycline, were seeded as described above, and treated overnight with  $60 \mu\text{mol/L}$  chloroquine (vesicular blocking; ref. 20). After 24 hours, fixative solution (2.5% glutaraldehyde in cacodylate buffer  $0.1 \text{ mol/L}$  pH 7.4) was added for 2 hours. The samples were then stored in cacodylate buffer at  $4^\circ\text{C}$ . Cells were then post fixed with a solution of 1% osmium tetroxide in  $0.1 \text{ mol/L}$  cacodylate buffer and embedded in epoxy resins after a graded-acetone serial dehydration step. Ultrathin slices of  $100 \text{ nm}$  were stained by uranyl acetate solution and lead citrate, and then analyzed by a transmission electron microscope, CM10 Philips (FEI Company) at an accelerating voltage of  $80 \text{ kV}$ . Images were recorded with a Megaview III Digital Camera (FEI Company).

#### Bioinformatic analysis

Neuroblastoma arrays were downloaded (E-MTAB-1781) and normalized. Briefly, mitochondrial involved genes were selected from gene ontology (GO) and the literature and used to train a self-organizing map and to cluster patient gene expression profiles. Survival and differential expression gene analyses were applied on the two found clusters. A self-organizing map and random forest model were used to perform feature selection to build a score. ClueGO application was used to find pathway enrichment networks differentially present in the two clusters. The genes in the reactive oxygen species (ROS) and Mitophagy pathway lists were obtained from the ClueGO analysis. A detailed description is presented for the bioinformatic data in the Supplementary Materials and Methods (Supplementary Data).

#### ROS measurement

Kelly and Tet21N cell lines were seeded as described above. After 48 hours, the glass support on which the cells were cultured were stained with 2',7'-dichlorofluorescein diacetate (DCFDA; Sigma-Aldrich) and MitoSOX Red Mitochondrial Superoxide Indicator (M36008, Thermo Fisher Scientific) according to the manufacturer's instructions. Cells were fixed as described above and analyzed by confocal microscopy. The acquired data were processed by the ImageJ processing program. Kelly cells were treated as described above, detached, stained with DCFDA, and subjected to flow cytometry with the CytoFLEX cytometer (Beck-

man Coulter) for ROS quantification. Data were analyzed using FlowJo software.

#### Neuroblastoma luminescent cells

Phoenix-Ampho cells were transfected with Lipofectamine 2000 (Invitrogen) and plasmid pMMP-Lucneo (kindly provided by Professor Andrew Kung, Harvard Medical School, Boston, MA). The viral particles were collected at 48 and 72 hours after transfection. The Kelly cell line was spinoculated with the viral particles and polybrene (hexadimethrine bromide, Sigma). The cells were subjected to selection for 15 days with  $1 \text{ mg/mL}$  of G418 (Calbiochem). The best cell clones were selected and their luminescence was measured. The resulting cell line was named Kelly-*luc*.

#### Xenograft ectopic neuroblastoma mouse model

All experiments were approved by the Scientific Ethical Committee of Bologna University (protocol no. 07/73/2013 and 564/2018-PR). Four- to 6-week-old NOD/SCID CB17 mice of both sexes were inoculated with  $10 \times 10^6$  Kelly-*luc* cells in Corning Matrigel Matrix. Mice were sedated with isoflurane prior to the injection. The pellet was inoculated by injection in the dorso-posterior-lateral position. The growth of the tumor was evaluated by luminescence acquisition. D-Luciferin was administered by intraperitoneal injection. Luminescence was acquired by the UviTec Imaging System (Uvitec). Treatment was performed after the tumor reached the predefined starting point in the bioluminescent acquisition. PNA oligo was then administered to the treatment group every day for 14 days. The animals were sacrificed at day 15. The tumors were removed, measured, weighed, and fixed in 4% formalin. For the event-free survival curve, mice were treated daily with a dorsal subcutaneous injection of  $100 \mu\text{L}$  of vehicle or BGA002 ( $10 \text{ mg/kg/day}$ ) for 28 days. Animals were monitored once every other day for tumor diameter measurement (using a caliper) and total tumor volume was extrapolated. An endpoint of at least  $10 \text{ mm}$  tumor diameter and a total tumor volume of  $523 \text{ mm}^3$  were established.

#### IHC

The neuroblastoma tumors were dehydrated, embedded in paraffin, and cut into  $4\text{-}\mu\text{m}$  sections. Paraffin removal was accomplished by incubating histologic slides in toluene followed by incubation in ethanol. The slides were incubated in 2%  $\text{H}_2\text{O}_2$  methanol for inhibition of endogenous peroxidase activity. Hydration was performed by serial incubation with 96% ethanol, 70% ethanol, and distilled water. Antigen retrieval was performed by heat processing in  $1 \text{ mmol/L}$  EDTA, pH 8, for N-Myc antibody, and in  $10 \text{ mmol/L}$  citrate pH 6 for TRAP1. The slides were blocked with 10% BSA in PBS, stained with the N-Myc (OP13, Calbiochem), Ki-67 (MIB1, Dako), and TRAP1 (TR1, Santa Cruz Biotechnology) antibodies and subsequently treated with secondary antibody (anti-mouse, Dako). The peroxidase coloration reaction was performed using the Dako DAB Kit. The slides were stained with hematoxylin, dehydrated, and mounted. Images were acquired with the Leitz Diaplan microscope.

#### Statistical analysis

Statistical analysis was performed with the Prism software version 6 (GraphPad) or with R software version 3.5. Python software version 3.0 was used to perform t-SNE. The different analyses and tests were specifically designed for each experiment.

## Results

### BGA002 is a novel MYCN-specific antigene oligonucleotide with potentially improved MYCN transcriptional inhibition

We have previously reported the effect of an MYCN-specific antigene PNA (agPNA) oligonucleotide (BGA001) for the selective inhibition of MYCN in neuroblastoma cell lines. This inhibition led to decreased transcription, reduced cell viability, and apoptosis (16). Furthermore, the MYCN agPNA was able to inhibit MYCN transcription in rhabdomyosarcoma cell lines, which led to antitumor activity *in vivo* in mice (17). Thus, our first aim was to compare the effects of the novel MYCN-specific agPNA oligonucleotide (BGA002) with the previous one (BGA001). BGA002 was conjugated to a nuclear localization signal peptide for delivery (16, 21, 22), because it was previously found to facilitate the penetration of BGA001 into cells, without requiring a transfection agent, and localization to the nucleus. Indeed, BGA002 showed potentially enhanced activity in downregulating MYCN mRNA expression in comparison with the agPNA BGA001 in MNA neuroblastoma cells (Fig. 1A). Moreover, BGA002 was much more efficient in reducing cell viability and N-Myc protein degradation than BGA001 (Fig. 1B and C), and in inducing apoptosis at 24 and 48 hours (Fig. 1D; Supplementary Fig. S1A). Therefore, as demonstrated by the EC<sub>50</sub> comparison, BGA002 shows a stronger antitumor effect *in vitro* in comparison with the previous agPNA (Supplementary Table S3).

To evaluate the *in vitro* activity of BGA002 in neuroblastoma, we selected a panel of 20 cell lines to cover the broad landscape of neuroblastoma tumors: MNA cell lines ( $n = 10$ ), MNA/p53<sub>mut</sub> ( $n = 4$ ), not-MNA ( $n = 5$ ), and not-MNA/p53<sub>mut</sub> ( $n = 1$ ). All the selected neuroblastoma cell lines showed expression of MYCN mRNA, with consistently higher levels detected in MNA cell lines (Supplementary Fig. S2A). BGA002 shows a strong dose-dependent inhibitory effect on MYCN transcription and on cell viability (Fig. 1E and F; Supplementary Fig. S2B and S2D). MNA cell lines were significantly more susceptible to the effects of BGA002 as demonstrated by a lower EC<sub>50</sub> compared with the MNA/p53<sub>mut</sub> cell line (Fig. 1F).

As expected, BGA002 was MYCN specific and did not influence cell viability in the MYCN-unexpressed HEK293 cells (Supplementary Fig. S3A), whereas a mutated version of BGA002 (BGA002<sub>mut</sub>) did not have any effect on MYCN transcription (Supplementary Fig. S3B), on cell viability of MYCN-expressing MNA neuroblastoma cells (Supplementary Fig. S3C), on N-Myc downstream targets (Supplementary Fig. S3D), and on inducing apoptosis (Supplementary Fig. S3E and S3F). Moreover, BGA002 bound to the unique target DNA sequence in the MYCN gene, whereas BGA002<sub>mut</sub> showed no binding (Supplementary Fig. S3G).

### Specific MYCN inhibition by BGA002 leads to profound mitochondrial damage in MNA neuroblastoma cells

Because MYCN mRNA inhibition persisted at 48 hours (Supplementary Fig. S2C), at which time we found extensive apoptosis levels (Fig. 1D), we decided to perform transmission electron microscopy to investigate the leading cause of this phenomenon. Ultrastructural analysis showed that MYCN inhibition by BGA002 caused profound mitochondrial changes in MNA neuroblastoma cells. After 12 hours, we observed initial mitochondrial damage (Supplementary Fig. S4A) without concomitant

apoptosis (Supplementary Fig. S4B and S4C), suggesting that apoptosis is a consequence of the observed phenomenon, rather than the cause. After 48 hours (or 72 hours) of BGA002 treatment, the mitochondria had sustained extensive damage (Fig. 2A; Supplementary Fig. S5C) while at 24 hours we noticed that mitochondria became smaller and the cristae patterns were much less elaborate (Supplementary Fig. S5B). Indeed, mitochondrial alterations were not observed after treatment with a mutated control antigene PNA (BGA002<sub>mut</sub>), after 48 hours or at 72 hours (Supplementary Fig. S5A and S5C).

Generally, the distribution and connection pattern is indicative of mitochondrial mass and function (23, 24). Although MitoTracker staining reveals that in the untreated MNA neuroblastoma cells the mitochondria are highly interconnected, anti-MYCN BGA002 treatment disrupted these mitochondrial nets, and the mitochondrial content appears to be reduced (Fig. 2B; Supplementary Fig. S5D). Moreover, BGA002 induced a change in the mitochondrial pattern, resulting in a perinuclear distribution (Fig. 2B). As before, BGA002<sub>mut</sub> failed to affect the mitochondrial nets (Supplementary Fig. S5D). Interestingly, we observed much less mitochondrial damage and pattern alteration after 48 hours of BGA001 (Supplementary Fig. S6A and S6B). Furthermore, BGA002 treatment led to a decrease in the mitochondrial area per cell (25) in the MNA cells (Supplementary Fig. S7A), and we observed a BGA002 dose-dependent mitochondrial mass reduction after 48 and 72 hours of treatment (Supplementary Fig. S7B and S7C).

### Alterations in mitochondrial pathways can identify patients with neuroblastoma with poor survival prognosis

To verify the impact of mitochondrial gene signature on neuroblastoma prognosis, we selected genes from the GO mitochondrial pathways and from the available literature (1,718 genes; Supplementary Table S4). For this purpose, we used a publicly available dataset that included patient clinical annotations (26). We used the mitochondrial-related signature to conduct a self-organization map to separate gene expression profiles from neuroblastoma in two different clusters of patients (Fig. 3A–C; Supplementary Fig. S8A; Supplementary Table S5). The two clusters have a statistically significant difference in the overall survival rates and event-free probability (Fig. 3D; Supplementary Fig. S8B), with cluster 2 strongly linked with a poor survival prognosis. Indeed, cluster 2 shows a similar worsening of the overall survival probability for the MNA patient subgroup (Fig. 3E). We further investigated which genes had a larger effect on event-free and overall survival. For this purpose, we used a random forest model optimized for censored data to conduct feature selection. The variables extracted from the model and from the self-organization map were used to construct a MitoScore. The top 200 genes qualifying for MitoScore are shown in word cloud (Fig. 3F; Supplementary Fig. S8C; Supplementary Table S6). The genes present in MitoScore and differentially expressed in the two clusters (Supplementary Table S7) were used to identify which functional pathways were linked to each cluster. Filtering the insignificant pathways, we found 20 GO pathways specific for cluster 1 and 45 for cluster 2 (Fig. 3G; Supplementary Tables S8 and S9). As expected, analysis highlighted the presence of a substantial number of folic acid pathway genes in cluster 2, because it is known that MYCN-amplified neuroblastomas have an enhanced dependency on folate (27). Moreover, cluster 2 contains a number of genes in response to ROS genes

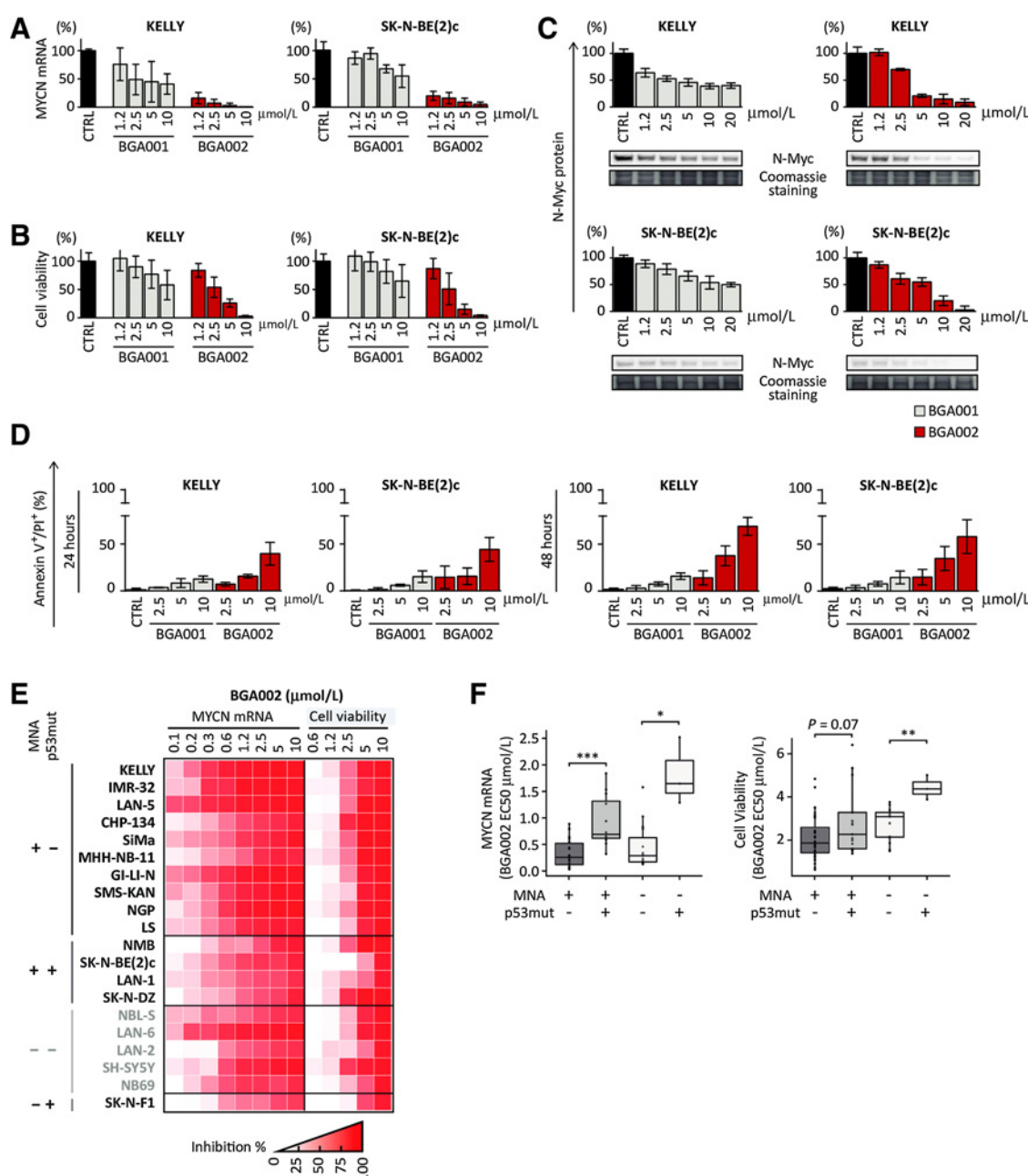


**Figure 1.**

BGA002 is a new specific anti-MYCIN antigene oligonucleotide with potently improved MYCN transcription inhibition properties leading to cell-growth inhibition and apoptosis in neuroblastoma cells. **A–E**, Comparison of the *in vitro* efficacy between neuroblastoma cells [Kelly and SK-N-BE(2)c] treated with different doses of BGA001 and BGA002. Bars, mean; whiskers, SD. **A**, MYCN mRNA expression inhibition through RT-PCR after 12 hours of treatment, BGA001 (gray) and BGA002 (red;  $n = 3$ , biological replicates for each cell line). **B**, Cell viability assay showing a decrease after 72 hours of treatment, BGA001 (gray) and BGA002 (red;  $n = 3$ , biological replicates for each cell line). **C**, Representative Western blot analysis of N-Myc after 24 hours. Representative staining for N-Myc (top) and whole-lane Coomassie staining (bottom) is shown. Top, quantification of N-Myc expression (normalized with Coomassie staining). Bars, mean; whiskers, SD ( $n = 2$ , biological replicates for each cell line). Left, BGA001; right, BGA002. First line, Kelly cell line; second line, SK-N-BE(2)c. **D**, Bar represents the percentage of cells stained by Annexin V<sup>+</sup>/PI<sup>+</sup> for the cell line treated for 24 (left) or 48 hours (right;  $n = 3$ , biological replicates for each cell line). **E**, Heatmap representing different neuroblastoma cell lines treated with different doses of BGA002. MYCN mRNA expression inhibition through RT-PCR (left) after 12 hours of treatment and a decrease in cell viability after 72 hours of treatment (right). The red scale represents the average percentage of inhibition of different biological replicates for each cell line ( $n = 3$ ) normalized to the control. **F**, mRNA MYCN inhibition (left) and vitality decrement (right) EC<sub>50</sub> for each cell line grouped according to MYCN amplification and/or p53 mutation. Each dot represents a singular experiment ( $n = 3$  for each cell line). Each point represents an individual sample; middle line indicates the median; box limits indicate the first and third quartiles; the whiskers indicate samples within 1.5 times the interquartile range. Wilcoxon matched pair test; \*,  $P < 0.05$ ; \*\*,  $P < 0.01$ ; \*\*\*,  $P < 0.001$ .

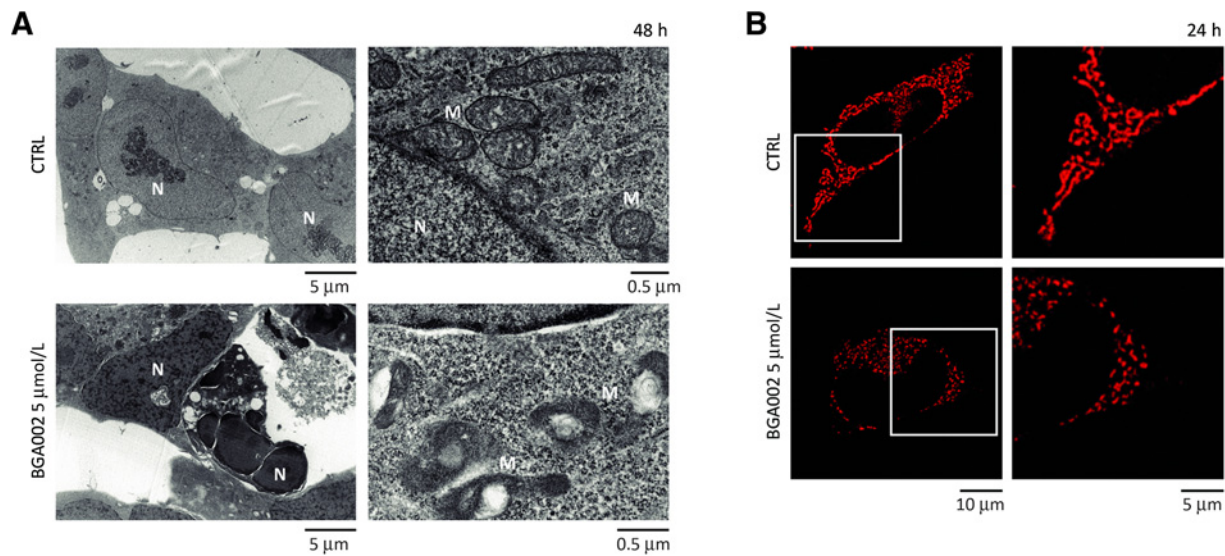


**Figure 2.**

BGA002 leads to MYCN-specific structural and functional alterations in mitochondria in MNA neuroblastoma cells. **A**, Transmission electron micrographs of the Kelly cell line treated for 48 hours with 5  $\mu\text{mol/L}$  BGA002. Untreated cells are shown in the first row; BGA002-treated cells are shown in the second row. M, mitochondrion; N, nucleus. **B**, Evaluation of mitochondrial nets in the Kelly cell line treated for 48 hours with 5  $\mu\text{mol/L}$  BGA002.

(RROS; Fig. 3G; Supplementary Table S9). Conversely, we found that cluster 1 contained a significant number of genes related to mitophagy (Fig. 3G; Supplementary Table S9). On the basis of pathway analysis, we built an RROS score and a mitophagy score. The high presence of genes related to response to ROS was significantly predictive for overall survival. It was also noted that a lower number of genes present related to mitophagy significantly worsened the overall survival probability (Fig. 3H). The RROS and mitophagy scores showed significant inverse correlation (Pearson coefficient =  $-0.73$ ,  $P = 2.2e-16$ ). Interestingly, the presence of MYCN correlated well with the RROS score ( $0.63$ ,  $P = 2.2e-15$ ) and showed inverse correlation with the mitophagy score ( $-0.73$ ,  $P = 2.2e-16$ ; Supplementary Fig. S8E). Ultimately, it was noted that the results from MYCN-amplified patients showed a substantial presence of mitochondrial related signature genes and a higher RROS score in comparison with patients lacking MYCN amplification (Supplementary Fig. S9A).

#### BGA002 reverts N-Myc–dysregulated mitochondrial pathways in MNA neuroblastoma

MYCN alteration of the transcriptional program is critical in promoting tumorigenesis in MNA neuroblastoma. Given this view, we investigated the effects of MYCN inhibition by BGA002 on gene-expression profiles in several neuroblastoma cell lines. As expected, genes present in the mitochondrial signature, and with a high score, show different expression levels between clusters 1 and 2 (Fig. 4A). Surprisingly, we found the same behavior in MYCN-amplified versus MYCN-nonamplified patients (Fig. 4A). Furthermore, we noticed that these genes are significantly predictive for overall survival (Fig. 4B). We also found that different genes in the mitochondrial signature correlate well or show inverse correlation with MYCN in the data set of patient gene expression profiles (Fig. 4C). On the basis of these results, we investigated whether MYCN inhibition by BGA002 was able to downregulate genes

from the mitochondrial signature (Fig. 4D). MYCN inhibition led to the downregulation of a wide group of mitochondrial genes in the different neuroblastoma cell lines. MYCN silencing by BGA002 also downregulated other previously described MYCN-related genes (Fig. 4D), including *TERT* and *SKP2* (28, 29). The use of an anti-MYCN siRNA and the Tet21N cells (in which inducible MYCN silencing is achieved by tetracycline administration, but not by BGA002, because these cells lack the agPNA target sequence in the inserted MYCN construct; Supplementary Fig. S10A; ref. 30) as controls, resulted in the same gene expression pattern (Fig. 4D). Interestingly, by confirming MYCN correlation with a response to ROS and an inverse correlation with mitophagy as previously shown, we found that MYCN inhibition downregulated the gene expression of TRAP1 while upregulating the expression of OPTN (Fig. 4D). These genes are involved in mitochondrial ROS control and in mitophagy, respectively (31–33). We also confirmed mitochondrial protein production variation in MNA neuroblastoma cells, a concomitant decrease in TRAP1, and an increase in OPTN production (Fig. 4E). Moreover, TRAP1 decrease and OPTN increase are accentuated at 48 hours (Fig. 4E). Based on our finding that MYCN shows inverse correlation with the mitophagy score in neuroblastoma and on the well-described important positive role of OPTN in this pathway (32), we investigated the inhibitory role of MYCN on mitophagy activation. In Tet21N cells after MYCN silencing (72 hours of tetracycline administration) while not observing apoptosis (Supplementary Fig. S10B and S10C), we registered a dramatic decrease in mitochondrial number (Supplementary Fig. S10D). Concomitantly, we observed the appearance of a high number of myelin figures (Fig. 4F) and colocalization of mitochondria with lysosomes (Supplementary Fig. S10E). Collectively, these findings are indicative of mitophagy activity after MYCN inhibition. Finally, an siRNA anti-OPTN significantly reduced mitophagy activity after MYCN silencing in Tet21N cells (Supplementary Fig. S11A–S11D).

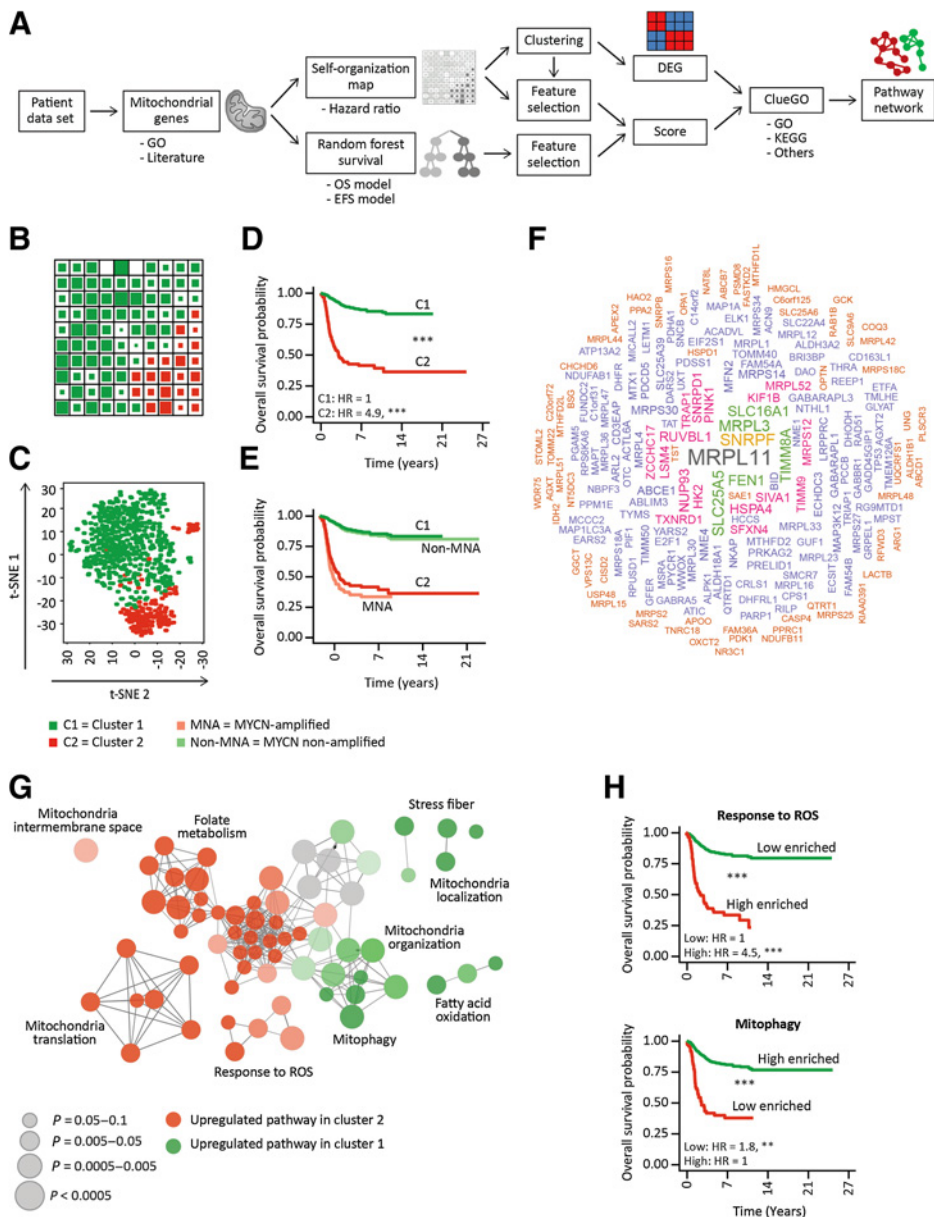


**Figure 3.**

Alterations in mitochondrial pathways identify patients with neuroblastoma with poor survival prognosis. **A**, Schematic representation of the bioinformatic pipeline analysis conducted. A dataset of neuroblastoma gene expression profiles was downloaded. Genes selected from the literature or listed in GO as part of the mitochondrial-associated terms were used to generate a mitochondrial-related signature. A self-organization map was utilized to associate patient gene expression profiles with two different clusters with a different survival probability. The genes in the mitochondrial-related signature were ranked by their contribution to the separation of patient gene expression profiles in two different clusters. Their contributions to predicting overall survival and event-free survival were also taken into account to build a MitoScore for all the genes present in the mitochondrial-related signature. We used genes in the MitoScore that were differentially expressed to build a functional grouped network of pathways. **B**, Heatmap showing the two different clusters (cluster 1, green; cluster 2, red) derived from the self-organization map. Each square represents a neuron; the size of the inner square is proportional to the number of patient gene expression profiles associated with that neuron. **C**, T-distributed stochastic neighbor embedding (t-SNE) showing the clustering of the transcriptional profiles (considering the genes present in the mitochondrial-related signature) of the patient gene expression profiles. Each dot represents a patient transcriptional profile; the dots are colored according to which cluster they belong to [cluster 1 ( $n = 541$ ), green; cluster 2 ( $n = 122$ ), red]. **D**, Kaplan-Meier plots for the probability of overall survival over time for patients associated with cluster 1 (green;  $n = 541$ ) and cluster 2 (red;  $n = 161$ ). Associated  $P$  value (log-rank test) is shown in the middle. HR and associated  $P$  value (log-rank test) are shown at the bottom left of the plot. **E**, Kaplan-Meier plots for the probability of overall survival over time for patients associated with cluster 1 (green) and cluster 2 (red), MNA patient (light green;  $n = 122$ ) and non-MNA patient (light red;  $n = 580$ ). **F**, Word cloud of the top 200 genes ranked by MitoScore; the size is proportional to the associated MitoScore. **G**, Functional grouped network of the pathways upregulated in cluster 1 (green) and cluster 2 (red). Circle size is proportional to the  $P$  value (FDR < 0.05). **H**, Kaplan-Meier plots for the probability of overall survival over time for patients associated with response to ROS score (low enriched,  $n = 614$ ; high enriched,  $n = 88$ , top) and mitophagy score (low enriched,  $n = 73$ ; high enriched,  $n = 629$ , bottom).  $P$  value associated with the curve is shown in the middle of the plot (log-rank test). Hazard ratio and associated  $P$  value (log-rank test) are shown at the bottom left of the plot. \*\*,  $P < 0.01$ ; \*\*\*,  $P < 0.001$ .

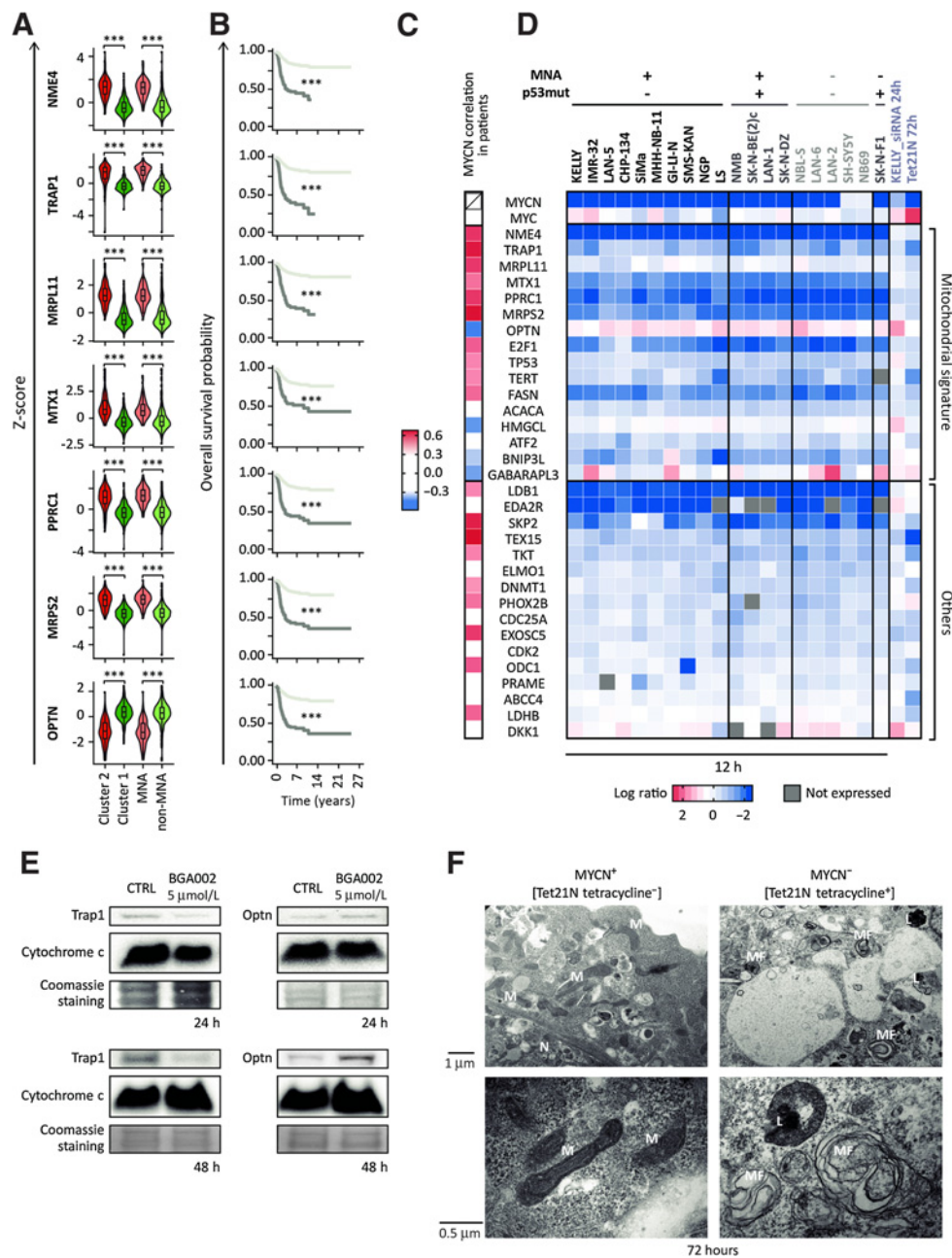


**Figure 4.** Blocking of MYCN leads to MYCN-specific gene expression signature inhibition in neuroblastoma cells and to mitophagy reactivation. **A**, Expression of different genes presented in the mitochondrial-related signature in cluster 2, cluster 1, MNA, and non-MNA patient gene expression profiles and presented as z-scores. Each point represents an individual sample; middle line indicates the median; the whiskers indicate samples within 1.5 times the interquartile range (statistical test, Wilcoxon). **B**, Kaplan–Meier plots for the probability of overall survival over time for patients associated with different genes present in the mitochondrial-related signature. For *NME4*, *TRAP1*, *MRPL11*, *PPRC1*, *MRPS2*, the dark gray line represents a z-score > 1, for *OPTN*, a z-score < –1. Hazard ratio and *P* value (log-rank test) are shown at the bottom left of the plot. **C** and **D**, Gene names in the middle refer to both panels. **C**, Color scale represents Pearson correlation coefficient of genes present in the mitochondrial-related signature (top) and other N-Myc targets (bottom) with MYCN in the patient gene expression profile data set. **D**, Heat map of the gene expression variation in neuroblastoma cell lines (MNA, MNA/p53-mut, non-MNA, and non-MNA/ p53-mut) after 12 hours of BGA002 treatment (5 μmol/L). On the right side of the heat map, Kelly cells treated with anti-MYCN siRNA and Tet21N cells treated with tetracycline (72 hours) are shown. The color scale represents the log<sub>2</sub>-fold change in comparison with the untreated cell line (*n* = 2 for each cell line). Gray, gene not expressed. Top, genes present in the mitochondrial-related signature; bottom, other N-Myc targets. **E**, Western blot analysis for TRAP1 (left, top row) and OPTN (right, top row), cytochrome c (middle row), and Coomassie staining (bottom row) of Kelly untreated cells and BGA002 (5 μmol/L)-treated cells for 24 (first line) and 48 hours (second line). **F**, Transmission electron micrographs of Tet21N cultured cells treated without (first line) and with (second line) tetracycline and chloroquine for 72 hours. From left to right, increasing magnification. M, mitochondrion; MF, myelin figure; L, lysosome; N, nucleus. \*\*\*, *P* < 0.001.

Downloaded from <http://aacrjournals.org/cancerres/article-pdf/79/24/6166/2786628/6166.pdf> by guest on 21 February 2024

**BGA002 leads to loss of protective N-Myc effect against mitochondrial ROS through TRAP1 downregulation in MNA neuroblastoma**

On the basis of our finding of a positive correlation between MYCN expression and the RROS score in the poor survival prognosis cluster 2 from the neuroblastoma patient dataset (Supplementary Fig. S8E), we investigated whether MYCN inhibition by BGA002 could induce augmentation of mitochondrial ROS production. Indeed, BGA002 treatment induced upregulation of the ROS and an increase in superoxide production (Fig. 5A; Supplementary Fig. S12A). Because TRAP1 plays a determining role in mitochondrial ROS control and considering that BGA002 treatment downregulated *TRAP1* expression, we investigated whether TRAP1 inhibition led to an increment in ROS production in MNA neuroblastoma. Indeed, siRNA against *TRAP1* (siTRAP1) led to an increment in production of ROS in mitochondria (Fig. 5A). TRAP1 downregulation by siTRAP1 also inhibited the mitochondrial net structure (Fig. 5B), similar to MYCN inhibition

after BGA002 treatment. Moreover, siTRAP1 consistently reduced cell viability (Fig. 5C). As a control, we verified that siTRAP1 did not affect MYCN mRNA expression (Fig. 5D). Interestingly, in Tet21n cells, which showed mitophagy reactivation after MYCN silencing (by tetracycline administration) and did not undergo apoptosis, we did not find an appreciable increase in ROS production (Supplementary Fig. S12B). Moreover, BGA002<sub>mut</sub> failed to induce ROS production, whereas BGA001 showed a modest effect (Supplementary Fig. S12C), and the latter did not consistently reduce *TRAP1* mRNA expression (Supplementary Fig. S12D). This mechanism is graphically represented in Supplementary Fig. S13A.

**BGA002 causes elimination of MNA neuroblastoma in mice**

Finally, we evaluated the *in vivo* antitumor activity of BGA002 in a xenograft murine model of MNA neuroblastoma. We inoculated MNA neuroblastoma Kelly-luminescent cells, which were monitored until tumor luminescence was detectable. Treatment

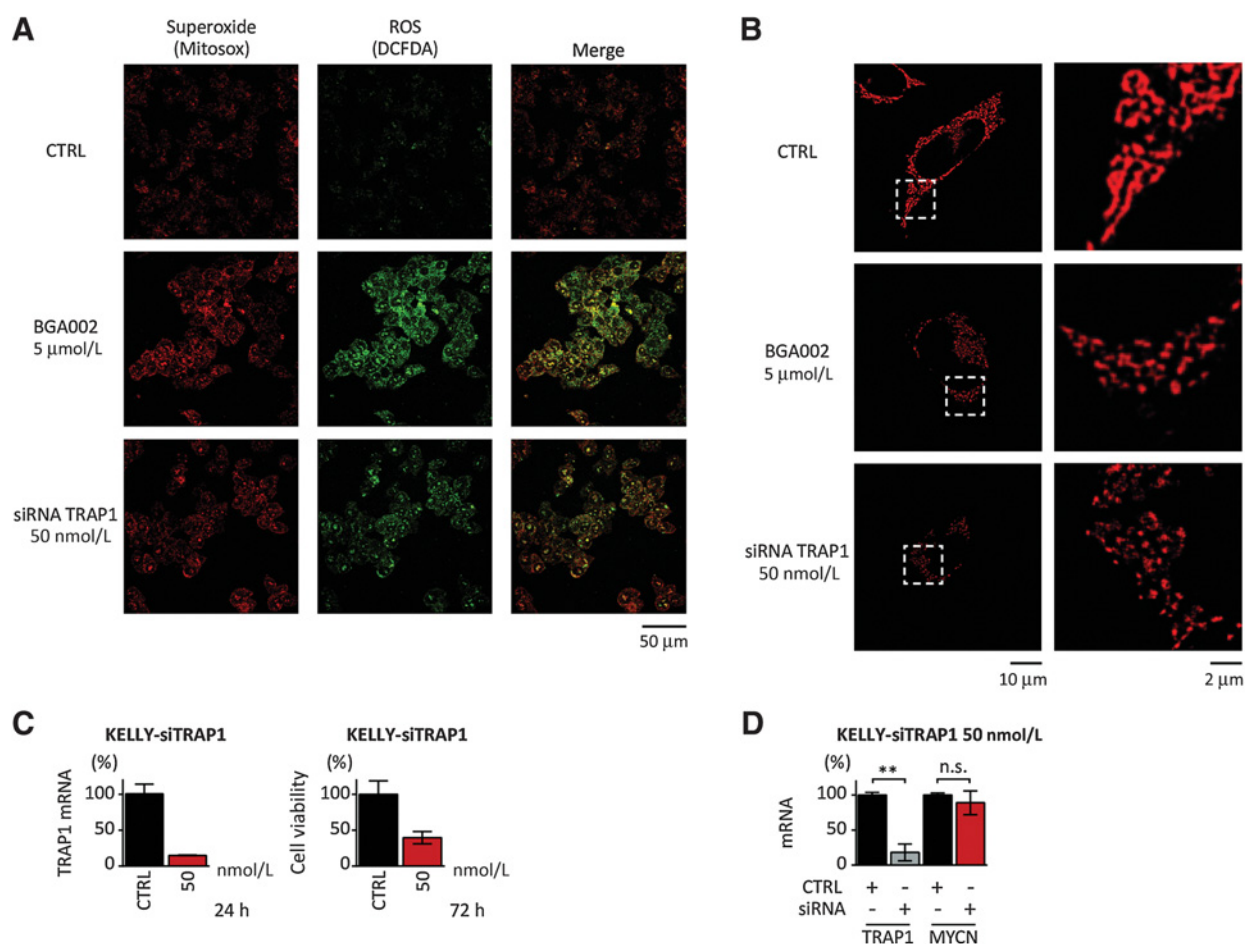


**Figure 5.** BGA002 reverts the MYCN control of ROS generation by *TRAP1* downregulation in MNA neuroblastoma cells. **A**, Representative confocal microscopy analysis of ROS production in Kelly untreated cells (top), Kelly cells treated with 5 μmol/L BGA002 (middle) for 48 hours, and Kelly cells treated with anti-*TRAP1* siRNA (bottom) for 24 hours. Mitosox staining, red (left); DCFDA staining, green (middle); merge (right). From left to right, increasing magnification. **B**, Evaluation of mitochondrial nets in the Kelly cell line treated for 48 hours with vehicle (top), with 5 μmol/L BGA002 (middle), and 50 nmol/L anti-*TRAP1* siRNA (bottom). From left to right, increasing magnification. **C**, Kelly cell line treated with 50 nmol/L siRNA anti-*TRAP1*. Left, *TRAP1* percentage of mRNA inhibition after 24 hours; right, percentage of cell viability inhibition ( $n = 2$ ) after 72 hours. **D**, Kelly cell line treated with 50 nmol/L siRNA anti-*TRAP1*, *TRAP1*, and MYCN, showing the percentage of mRNA inhibition after 24 hours ( $n = 3$ ). \*\*,  $P < 0.01$ ; n.s., nonsignificant.

with BGA002 resulted in a statistically significant augmentation of survival in comparison with the vehicle (Fig. 6A; Supplementary Fig. S13B).

Moreover, the subcutaneous administration (daily for 15 days) of BGA002 resulted in a potent and dose-dependent antitumor activity. BGA002 at 2.5 mg/kg/day caused a tumor weight decrease of 25%, whereas the treatment with 5 mg/kg/day resulted in a significant decrease of more than 70%, and administration at 10 mg/kg/day led to tumor elimination (Fig. 6B). We concluded that treatment with BGA002 showed a dose-response tumor growth inhibition.

After treatment with BGA002 at the intermediate dose (5 mg/kg/day), histologic analysis revealed a consistent reduction in tumor vascularization as compared with the vehicle group (Fig. 6C), whereas IHC analysis showed a consistent reduction in N-Myc protein staining and a decrease in Ki-67, leading to reduced TRAP1 protein expression (Fig. 6C).

### Discussion

The critical role of N-Myc in cancer development and its association with poor survival prognosis is not restricted to neuroblastoma, with a broad range of tumors available in which MYCN amplification and overexpression play a crucial role (34). Due to the highly restricted pattern of expression of MYCN in normal cells, N-Myc represents an optimal target for tumor-specific therapy for MYCN-expressing tumors.

Although the direct targeting of the N-Myc transcription factor protein is still challenging, antigene therapy by targeting MYCN transcription has great potential in treating MYCN-expressing tumors, as we previously demonstrated in the preclinical treatment of neuroblastoma and rhabdomyosarcoma by an MYCN-specific antigene PNA (16, 17).

Here, we report, for the first time, the preclinical results for BGA002, a novel MYCN-specific agPNA with potentially improved ability to block MYCN transcription. The BGA002 sequence is

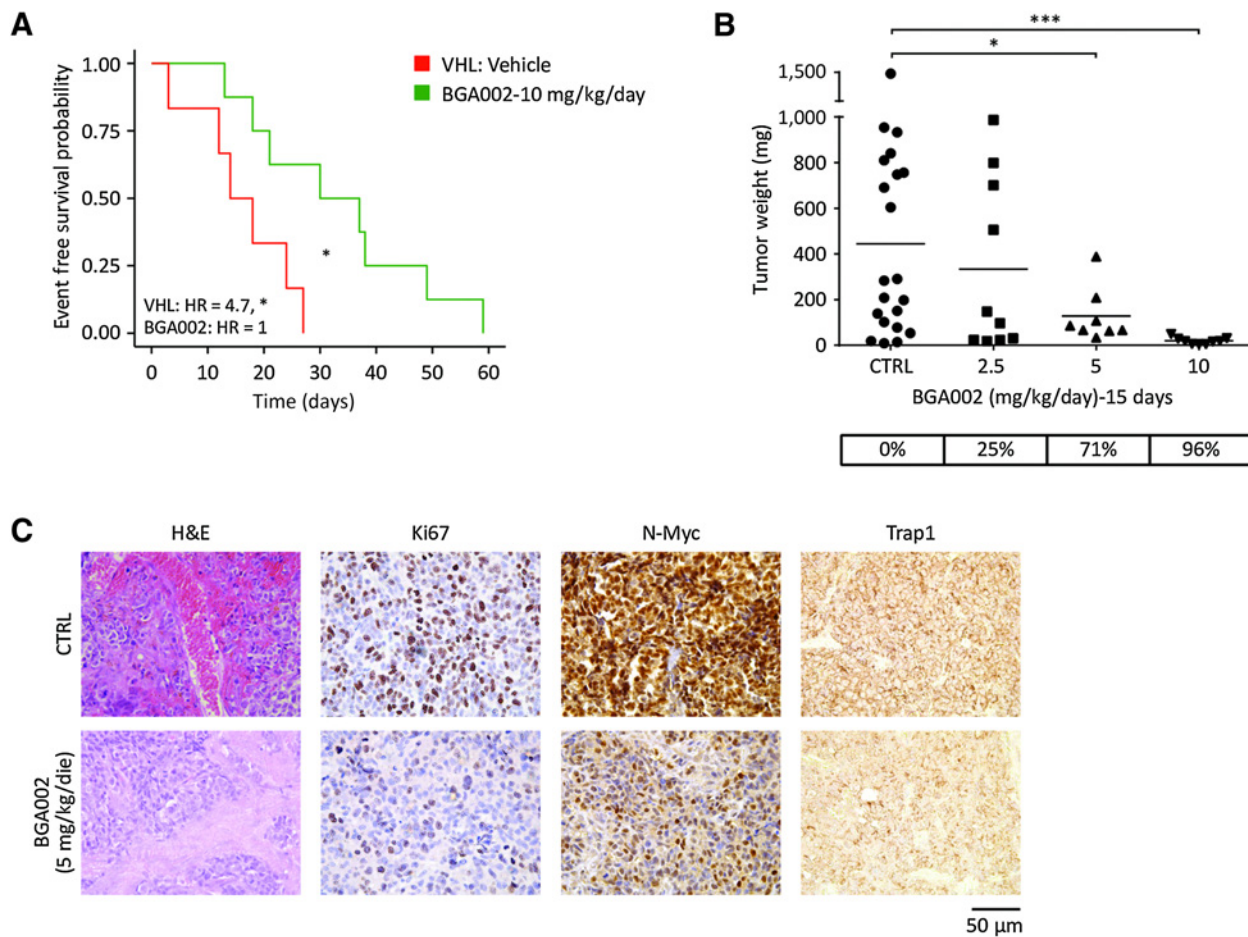


**Figure 6.** BGA002 causes elimination of MNA neuroblastoma in mice through TRAP1 downregulation. **A**, Kaplan-Meier plots for the probability of event-free survival over time for mice (Kelly-luc xenograft) treated with vehicle (red;  $n = 6$ ) and BGA002, 10 mg/kg/day (green;  $n = 8$ ). Middle, associated  $P$  value (log-rank test). Hazard ratio and associated  $P$  value (log-rank test) are shown at the bottom left of the plot. **B**, Evaluation of tumor weight in neuroblastoma xenograft mice treated with different doses of BGA002 [untreated ( $n = 21$ ), 2.5 ( $n = 11$ ), 5 ( $n = 8$ ), and 10 ( $n = 9$ ) mg/kg/day]. Each dot represents a mouse (Mann-Whitney test). The table below the graph indicates the mean value of tumor weight reduction for each treatment dose in comparison with the control. **C**, IHC analysis of neuroblastoma xenograft mice untreated (top) or treated with 5 mg/kg/day BGA002 (bottom). Images of sections are shown stained with hematoxylin and eosin (H&E; first column), Ki-67 antibody (second column), N-Myc antibody (third column), and TRAP1 antibody (fourth column). Similar results were obtained from four independent mice. \*,  $P < 0.05$ ; \*\*\*,  $P < 0.001$ .

complementary to a unique target sequence in the human (and mouse) MYCN gene. BGA002 showed dose-dependent inhibition of MYCN transcription and cell viability in a panel of 20 MYCN-expressing neuroblastoma cell lines with or without MNA. In comparison with BGA001, it showed a potently enhanced ability to specifically decrease MYCN mRNA and protein expression while decreasing the viability of neuroblastoma cell lines.

Interestingly, BGA002 is more effective in neuroblastoma cell lines with MNA versus p53-mutated or MYCN single copy cell lines. Because MYCN inhibition led to apoptosis, the higher EC<sub>50</sub> found in p53-mutated neuroblastoma cells could be explained by their higher resistance to apoptosis (35). MYCN inhibition led to the downregulation or upregulation of highly relevant genes involved in metabolism, cell-cycle control, apoptosis, metastasis, and DNA repair.

Surprisingly, the main ultrastructural alteration that we found in MNA neuroblastoma cells after MYCN inhibition was alteration of mitochondrial structure and organization. Interestingly, BGA001, which showed much less ability to induce mitochondrial alteration, exerted a lesser effect in the promotion of apoptosis. We also showed that a gene expression signature related to mitochondria allows for the identification of neuroblastoma patients with poor survival prognosis. Furthermore, we found that BGA002 treatment led to the downregulation or upregulation of different genes involved in this signature.

It is known that metabolic stress generally leads to autophagy (36), but its role in cancer is still controversial (37, 38). The impact of autophagy in neuroblastoma is also controversial (39) and depends on the p53 status of the cells (40). Moreover, mitophagy (a particular type of autophagy) is a fundamental process for mitochondrial turnover and health, and its deregulation can result in neurodegenerative disease and cancer insurgence (41, 42). Interestingly, we found that low enrichment in mitophagy-related genes is significantly predictive for a poor survival prognosis in a large data set of gene expression profiles from patients with neuroblastoma. Furthermore, we noticed that MYCN inhibition led to the upregulation of *OPTN*, which plays an important role in mitophagy induction (32, 33). Moreover, blocking MYCN expression in Tet21N cells led to the disappearance of mitochondria with concomitant presence of myelin figures, and colocalization of lysosomes with mitochondria, indicating mitophagy activation. This phenotype is significantly reduced after siRNA anti-*OPTN* administration, indicating that N-Myc blocks mitophagy through *OPTN* silencing.

ROS generation in mitochondria plays a role in cancer initiation, with many mitochondrial processes leading to ROS generation in tumor cells (43). Notwithstanding their role in tumorigenesis, ROS excess in cells leads to damage and ultimately to apoptosis (44). TRAP1 is a mitochondrial chaperone protein that plays a crucial role in mitochondrial homeostasis (31), and its downregulation corresponds to an increase in ROS presence, and to a higher susceptibility to oxidative stress (31). We found that inhibition of MYCN led to TRAP1 downregulation, an increase ROS generation, and induction of apoptosis in MNA neuroblastoma cells. Furthermore, BGA001 modestly reduced *TRAP1* expression and showed a less effective ability to induce ROS and promote apoptosis, indicating that N-Myc mitochondrial protection plays a relevant role in neuroblastoma.

There is a growing corpus of evidence that mitochondrial fate is connected to tumor formation and progression (45, 46). Neuroblastoma insurgence leads to profound metabolic changes, where

high-risk neuroblastoma shows a higher uptake of glucose and a reduction in oxidative phosphorylation in mitochondria (47). Although it has been claimed that N-Myc was involved in mitochondrial lipid metabolism in neuroblastoma (11), its role in mitochondrial regulation in neuroblastoma was largely unknown.

Here, we describe for the first time that N-Myc is relevant in mitochondrial structural maintenance and turnover. Our work highlights the prognostic value of mitochondrial dysregulation in neuroblastoma patients and provides a mechanism on how N-Myc controls previously unknown aspects of mitochondrial function, by inhibiting mitophagy, and controlling ROS generation.

Considering the role of N-Myc in a wide range of tumors, further studies on its close relationship with mitochondria will provide other valuable insights into cancer biology. Furthermore, considering the role of MYCN in mitochondrial ROS protection, it will be interesting to analyze the potential use of BGA002 in conjunction with other therapies that induce ROS in cancer cells.

BGA002 has received orphan drug designation from the Food and Drug Administration (orphan registry: DRU-2017-6085) and from the European Medicines Agency (orphan registry: EU/3/12/1016). Based upon its well-tolerated regulatory safety profile package, BGA002 is now moving to phase I clinical trials in neuroblastoma patients.

#### Disclosure of Potential Conflicts of Interest

R. Tonelli and A. Pession were unpaid consultant/advisory board members for BIOGENERA. No potential conflicts of interest were disclosed by the other authors.

#### Authors' Contributions

**Conception and design:** L. Montemurro, S. Raieli

**Development of methodology:** L. Montemurro, S. Raieli, S. Angelucci, D. Bartolucci, C. Amadesi, S. Lampis, L. Venturelli, G. Nieddu

**Acquisition of data (provided animals, acquired and managed patients, provided facilities, etc.):** L. Montemurro, S. Angelucci, D. Bartolucci, C. Amadesi, S. Lampis, M. Fischer

**Analysis and interpretation of data (e.g., statistical analysis, biostatistics, computational analysis):** S. Raieli, L. Venturelli, A. Pession

**Writing, review, and/or revision of the manuscript:** S. Raieli, L. Venturelli, M. Fischer, A. Pession, P. Hrelia, R. Tonelli

**Administrative, technical, or material support (i.e., reporting or organizing data, constructing databases):** L. Montemurro, D. Bartolucci, C. Amadesi, A.L. Scardovi

**Study supervision:** A. Pession, R. Tonelli

**Other (chemical synthesis):** G. Nieddu

**Other (synthesis of tested compound):** L. Cerisoli

**Other (samples preparation for TEM analysis and TEM images interpretation):** G. Teti

**Other (TEM analysis, interpretation, and writing of TEM data):** M. Falconi

#### Acknowledgments

We would like to thank Wissem Eljeder and Simone Maestri for suggestions and comments. We would also like to thank Andres E. Zucchetti from the Institut Curie for insightful suggestions on confocal microscopy analysis. R. Tonelli, A. Pession, and P. Hrelia are funded by the University of Bologna. G. Teti and M. Falconi are funded by the University of Bologna (Ricerca fondamentale orientata: RFO 2017, 2018) and by Fondazione del Monte di Bologna e Ravenna. L. Montemurro, S. Angelucci, and D. Bartolucci are funded by AGEOP. S. Raieli, C. Amadesi, S. Lampis, A. Scardovi, G. Nieddu, and L. Cerisoli are funded by BIOGENERA SpA.

The costs of publication of this article were defrayed in part by the payment of page charges. This article must therefore be hereby marked *advertisement* in accordance with 18 U.S.C. Section 1734 solely to indicate this fact.

Received January 3, 2019; revised July 10, 2019; accepted October 7, 2019; published first October 15, 2019.

## References

- Pinto NR, Applebaum MA, Volchenbom SL, Matthay KK, London WB, Ambros PF, et al. Advances in risk classification and treatment strategies for neuroblastoma. *J Clin Oncol* 2015;33:3008–17.
- Campbell K, Gastier-Foster JM, Mann M, Naranjo AH, Van Ryn C, Bagatell R, et al. Association of MYCN copy number with clinical features, tumor biology, and outcomes in neuroblastoma: a report from the Children's Oncology Group. *Cancer* 2017;123:4224–35.
- Weiss WA, Aldape K, Mohapatra G, Feuerstein BG, Bishop JM. Targeted expression of MYCN causes neuroblastoma in transgenic mice. *EMBO J* 1997;16:2985–95.
- Brodeur GM, Seeger RC, Schwab M, Varmus HE, Bishop JM. Amplification of N-myc in untreated human neuroblastomas correlates with advanced disease stage. *Science* 1984;224:1121–4.
- Seeger RC, Brodeur GM, Sather H, Dalton A, Siegel SE, Wong KY, et al. Association of multiple copies of the N-myc oncogene with rapid progression of neuroblastomas. *N Engl J Med* 1985;313:1111–6.
- Huang M, Weiss WA. Neuroblastoma and MYCN. *Cold Spring Harb Perspect Med* 2013;3:a014415.
- Matthay KK, Maris JM, Schleiermacher G, Nakagawara A, Mackall CL, Diller L, et al. Neuroblastoma. *Nat Rev Dis Primer* 2016;2:16078.
- Dang CV, Kim J, Gao P, Yuste J. The interplay between MYC and HIF in cancer. *Nat Rev Cancer* 2008;8:51–6.
- Qing G, Li B, Vu A, Skuli N, Walton ZE, Liu X, et al. ATF4 Regulates MYC-mediated neuroblastoma cell death upon glutamine deprivation. *Cancer Cell* 2012;22:631–44.
- Ruiz-Pérez MV, Henley AB, Arsenian-Henriksson M. The MYCN protein in health and disease. *Genes* 2017;8. doi: 10.3390/genes8040113.
- Zirath H, Frenzel A, Olynyk G, Segerström L, Westermark UK, Larsson K, et al. MYC inhibition induces metabolic changes leading to accumulation of lipid droplets in tumor cells. *Proc Natl Acad Sci U S A* 2013;110:10258–63.
- Zimmerman KA, Yancopoulos GD, Collum RG, Smith RK, Kohl NE, Denis KA, et al. Differential expression of myc family genes during murine development. *Nature* 1986;319:780–3.
- Fletcher JJ, Ziegler DS, Trahair TN, Marshall GM, Haber M, Norris MD. Too many targets, not enough patients: rethinking neuroblastoma clinical trials. *Nat Rev Cancer* 2018;18:389–400.
- Janowski BA, Kaihatsu K, Huffman KE, Schwartz JC, Ram R, Hardy D, et al. Inhibiting transcription of chromosomal DNA with antigene peptide nucleic acids. *Nat Chem Biol* 2005;1:210–5.
- Janowski BA, Huffman KE, Schwartz JC, Ram R, Hardy D, Shames DS, et al. Inhibiting gene expression at transcription start sites in chromosomal DNA with antigene RNAs. *Nat Chem Biol* 2005;1:216–22.
- Tonelli R, Purgato S, Camerin C, Fronza R, Bologna F, Alboresi S, et al. Antigene peptide nucleic acid specifically inhibits MYCN expression in human neuroblastoma cells leading to cell growth inhibition and apoptosis. *Mol Cancer Ther* 2005;4:779–86.
- Tonelli R, McIntyre A, Camerin C, Walters ZS, Leo KD, Selve J, et al. Antitumor activity of sustained N-Myc reduction in rhabdomyosarcomas and transcriptional block by antigene therapy. *Clin Cancer Res* 2012;18:796–807.
- Nielsen PE, Egholm M, Berg RH, Buchardt O. Sequence-selective recognition of DNA by strand displacement with a thymine-substituted polyamide. *Science* 1991;254:1497–500.
- Clayton DA, Shadel GS. Isolation of mitochondria from tissue culture cells. *Cold Spring Harb Protoc* 2014;2014. doi: 10.1101/pdb.prot080002.
- Dolman NJ, Chambers KM, Mandavilli B, Batchelor RH, Janes MS. Tools and techniques to measure mitophagy using fluorescence microscopy. *Autophagy* 2013;9:1653–62.
- Boffa LC, Cutrona G, Cilli M, Matis S, Damonte G, Mariani MR, et al. Inhibition of Burkitt's lymphoma cells growth in SCID mice by a PNA specific for a regulatory sequence of the translocated c-myc. *Cancer Gene Ther* 2007;14:220–6.
- Cutrona G, Carpaneto EM, Ulivi M, Roncella S, Landt O, Ferrarini M, et al. Effects in live cells of a c-myc anti-gene PNA linked to a nuclear localization signal. *Nat Biotechnol* 2000;18:300–3.
- Detmer SA, Chan DC. Functions and dysfunctions of mitochondrial dynamics. *Nat Rev Mol Cell Biol* 2007;8:870–9.
- Sauvanet C, Duvezin-Caubet S, di Rago J-P, Rojo M. Energetic requirements and bioenergetic modulation of mitochondrial morphology and dynamics. *Semin Cell Dev Biol* 2010;21:558–65.
- Vowinckel J, Hartl J, Butler R, Ralser M. MitoLoc: a method for the simultaneous quantification of mitochondrial network morphology and membrane potential in single cells. *Mitochondrion* 2015;24:77–86.
- Oberthuer A, Juraeva D, Hero B, Volland R, Sterz C, Schmidt R, et al. Revised risk estimation and treatment stratification of low- and intermediate-risk neuroblastoma patients by integrating clinical and molecular prognostic markers. *Clin Cancer Res* 2015;21:1904–15.
- Lau DT, Flemming CL, Gherardi S, Perini G, Oberthuer A, Fischer M, et al. MYCN amplification confers enhanced folate dependence and methotrexate sensitivity in neuroblastoma. *Oncotarget* 2015;6:15510–23.
- Evans L, Chen L, Milazzo G, Gherardi S, Perini G, Willmore E, et al. SKP2 is a direct transcriptional target of MYCN and a potential therapeutic target in neuroblastoma. *Cancer Lett* 2015;363:37–45.
- Nikiforov MA, Chandriani S, Park J, Kotenko I, Matheos D, Johnsson A, et al. TRRAP-dependent and TRRAP-independent transcriptional activation by Myc family oncoproteins. *Mol Cell Biol* 2002;22:5054–63.
- Wasylshen AR, Stojanova A, Oliveri S, Rust AC, Schimmer AD, Penn LZ. New model systems provide insights into Myc-induced transformation. *Oncogene* 2011;30:3727–34.
- Masgras I, Sanchez-Martin C, Colombo G, Rasola A. The Chaperone TRAP1 as a modulator of the mitochondrial adaptations in cancer cells. *Front Oncol* 2017;7:58.
- Moore AS, Holzbaur ELF. Dynamic recruitment and activation of ALS-associated TBK1 with its target optineurin are required for efficient mitophagy. *Proc Natl Acad Sci U S A* 2016;113:E3349–58.
- Richter B, Sliter DA, Herhaus L, Stolz A, Wang C, Beli P, et al. Phosphorylation of OPTN by TBK1 enhances its binding to Ub chains and promotes selective autophagy of damaged mitochondria. *Proc Natl Acad Sci U S A* 2016;113:4039–44.
- Rickman DS, Schulte JH, Eilers M. The expanding world of N-MYC-driven tumors. *Cancer Discov* 2018;8:150–63.
- Chesler L, Goldenberg DD, Collins R, Grimmer M, Kim GE, Tihan T, et al. Chemotherapy-induced apoptosis in a transgenic model of neuroblastoma proceeds through p53 induction. *Neoplasia* 2008;10:1268–74.
- Dikic I, Elazar Z. Mechanism and medical implications of mammalian autophagy. *Nat Rev Mol Cell Biol* 2018;19:349–64.
- Rybshtein MD, Bravo-San Pedro JM, Kroemer G, Galluzzi L. The autophagic network and cancer. *Nat Cell Biol* 2018;20:243–51.
- Wilde L, Tanson K, Curry J, Martinez-Otschoorn U. Autophagy in cancer: a complex relationship. *Biochem J* 2018;475:1939–54.
- Frentzel J, Sorrentino D, Giuriato S. Targeting autophagy in ALK-associated cancers. *Cancers* 2017;9. doi: 10.3390/cancers9120161.
- Mrakovcic M, Fröhlich LF. p53-mediated molecular control of autophagy in tumor cells. *Biomolecules* 2018. doi: 10.3390/biom8020014.
- Bordi M, Nazio F, Campello S. The close interconnection between mitochondrial dynamics and mitophagy in cancer. *Front Oncol* 2017;7:81.
- Palikaras K, Lionaki E, Tavernarakis N. Mechanisms of mitophagy in cellular homeostasis, physiology and pathology. *Nat Cell Biol* 2018;20:1013–22.
- Sabharwal SS, Schumacker PT. Mitochondrial ROS in cancer: initiators, amplifiers or an Achilles' heel? *Nat Rev Cancer* 2014;14:709–21.
- Murphy MP, Holmgren A, Larsson N-G, Halliwell B, Chang CJ, Kalyanaram B, et al. Unravelling the biological roles of reactive oxygen species. *Cell Metab* 2011;13:361–6.
- Sciacovelli M, Gonçalves E, Isaac Johnson T, Roberto Zecchini V, da Costa ASH, Gaude E, et al. Fumarate is an epigenetic modifier that elicits epithelial-to-mesenchymal transition. *Nature* 2016;537:544–7.
- Vyas S, Zaganjor E, Haigis MC. Mitochondria and Cancer. *Cell* 2016;166:555–66.
- Aminzadeh S, Vidali S, Sperl W, Kofler B, Feichtinger RG. Energy metabolism in neuroblastoma and Wilms tumor. *Transl Pediatr* 2015;4:20–32.